Theory of single-molecule controlled rotation experiments, predictions, tests, and comparison with stalling experiments in F_1-ATPase

Sándor Volkán-Kacsó[a] and Rudolph A. Marcus[a,1]

[a]Noyes Laboratory of Chemical Physics, California Institute of Technology, Pasadena, CA 91125

Contributed by Rudolph A. Marcus, August 26, 2016 (sent for review July 15, 2016; reviewed by Attila Szabo and Arieh Warshel)

A recently proposed chemomechanical group transfer theory of rotary biomolecular motors is applied to treat single-molecule controlled rotation experiments. In these experiments, single-molecule fluorescence is used to measure the binding and release rate constants of nucleotides by monitoring the occupancy of binding sites. It is shown how missed events of nucleotide binding and release in these experiments can be corrected using theory, with F_1-ATP synthase as an example. The missed events are significant when the reverse rate is very fast. Using the theory the actual rate constants in the controlled rotation experiments and the corrections are predicted from independent data, including other single-molecule rotation and ensemble biochemical experiments. The effective torsional elastic constant is found to depend on the binding/releasing nucleotide, and it is smaller for ADP than for ATP. There is a good agreement, with no adjustable parameters, between the theoretical and experimental results of controlled rotation experiments and stalling experiments, for the range of angles where the data overlap. This agreement is perhaps all the more surprising because it occurs even though the binding and release of fluorescent nucleotides is monitored at single-site occupancy concentrations, whereas the stalling and free rotation experiments have multiple-site occupancy.

F_1-ATPase | biomolecular motors | single-molecule imaging | nucleotide binding | group transfer theory

Single-molecule manipulation techniques, including stalling and controlled rotation methods or "pulling" force microscopies, have been used to augment imaging experiments in biomolecular motors (1–4). In F_1-ATPase, for example, beyond observing the kinetics of stepping rotation resolved into ∼80° and ∼40°substeps (5–7), the manipulation of the rotor shaft by magnetic tweezers recently opened up the possibility of directly probing the dynamical response of the system to externally constraining the rotor angle θ. In tandem with the experimental tools of X-ray crystallography (8) and ensemble biochemical methods (9), these experiments provide added insight into the processes in chemomechanical energy transduction (7, 10–13). The kinetic pathway along which concerted substeps occur in free rotation has been established (14), whereby binding of solution ATP to an empty subunit is initiated at $\theta = 0°$, and the release of hydrolyzed ADP from the clockwise neighboring subunit occurs simultaneously as the θ completes the ∼80° rotation step (Fig. 1). Using the detailed knowledge of individual substeps, stalling (3, 15) and controlled rotation (3) experiments provide an estimate of the rate constants of nucleotide binding and other processes as a function of θ. In particular, binding and release of ATP and analogs can be externally controlled to occur at angles other than 0°.

In the controlled rotation experiments (1, 4) we consider here, a slow constant angular velocity rotation of the shaft was produced by magnetic tweezers. A magnetic bead was attached to the rotor shaft protruding from the stator ring with a constant magnetic dipole moment pointing in the plane of the ring, the latter fixed to a microscope coverslip. An external magnetic field was created via permanent magnets and the magnetic bead aligned itself to the direction of this field. The direction of the external field was rotated in the plane of the stator ring, and the resulting change in the nucleotide occupancy was monitored using fluorescent ATP and ADP analogs, Cy3-ATP and Cy3-ADP. To permit individual observations, the solution was dilute in the nucleotide, resulting in a low site occupancy during single-molecule trajectories (4). Events whereby the occupancy σ changed between 0 and 1 were then analyzed; any higher occupancy events were excluded from the analysis. The number of binding $(0 \rightarrow 1)$ and release $(1 \rightarrow 0)$ events in narrow observation intervals of width $\Delta\theta$ was used to estimate forward $k_f(\theta)$ and backward $k_b(\theta)$ rate constants of nucleotide binding, respectively, also yielding the equilibrium constant $K(\theta) = k_f(\theta)/k_b(\theta)$.

In a previous article (16), we formulated a theory for treating the θ-dependent $k_f(\theta)$, $k_b(\theta)$, and $K(\theta)$ in stalling experiments and compared the predictions with the experimental data. In these experiments the rotor was stalled at some θ then released after a predetermined time, rather than rotated at a constant angular velocity. For the controlled rotation experiments, we consider several questions:

i) Are the results of stalling experiments and controlled rotation experiments consistent with each other and with a chemomechanical theory (16) of group transfer in the angular range where the two experiments overlap?

ii) Are the time resolution limitations of single-molecule fluorescence techniques used to monitor these events significantly leading to missed events, thus altering the outcome

Significance

The investigation of nucleotide binding and release dynamics vs. rotor shaft rotation in the F_1-ATPase enzyme is necessary to reveal biological function. We elucidate the mechanism of the exponential-like change of binding and release rate (and thus the equilibrium) constants when probed against the rotor angle at the single-molecule level. We extend our group transfer theory proposed for the stalling experiments to treat controlled rotation experiments. The model correctly predicts the controlled rotation data on fluorescent ATP without any adjustable parameters. The theory provides a framework able to treat the binding and release of various nucleotides. In the process we also learn about the properties of the fluorescent nucleotide Cy3-ATP.

Author contributions: S.V.-K. and R.A.M. designed research, performed research, analyzed data, and wrote the paper.

Reviewers: A.S., National Institutes of Health; and A.W., University of Southern California.

The authors declare no conflict of interest.

[1]To whom correspondence should be addressed. Email: ram@caltech.edu.

This article contains supporting information online at www.pnas.org/lookup/suppl/doi:10.1073/pnas.1611601113/-/DCSupplemental.

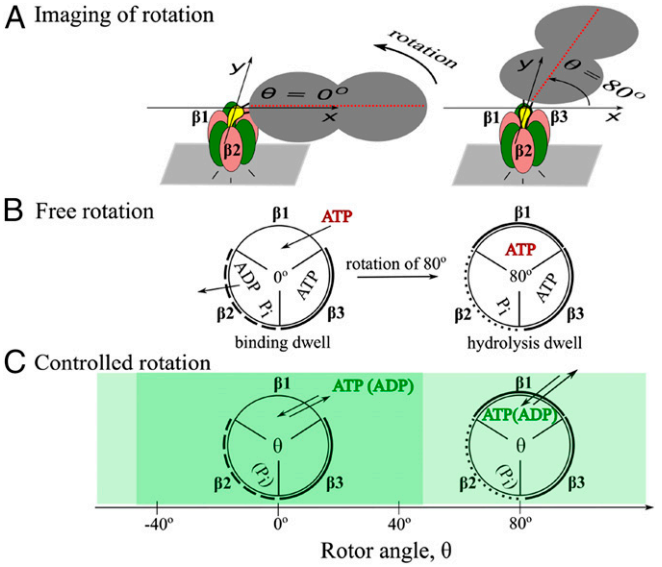

Fig. 1. Binding processes in F_1-ATPase imaged using a bead-duplex (*A*) for wild-type nucleotides in free rotation (*B*) and for fluorescent nucleotides in controlled rotation (*C*) experiments. The rotor (yellow γ subunit) is linked to the bead duplex with its major geometric axis (red dashed line) that defines the rotor angle θ relative to the *x* axis of the laboratory xy coordinate plane. Looking at the F_1-ATPase from the top (F_o side), θ increases counterclockwise. The coverslip (gray areas in *A*) to which the stator ring (green and pink α and β subunits) is fixed is in this xy plane. The range of $-50° < \theta < 50°$ is treated (dark shaded background in *C*) in which stalling experiments overlap with controlled rotation data (light shaded background). The species occupying the pockets of ring β subunits 1, 2, and 3 are shown at the dwell angles (0° and 80°), and the arrows indicate the displacement of the nucleotides during the 80°rotation. Thick arcs represent a closed subunit structure, and dashed and dotted lines indicate various degrees of openness.

of the rate measurements? If so, can one correct for such effects using theory?

iii) Is an approximation made in the analysis of the experiment of replacing the time spent in nonoccupied sites by the total trajectory time a significant approximation at any rotor angle value? If so, can one use theory to correct for this approximation?

iv) Can the theory predict the binding and release rate constants and their dependence on the rotor angle in F_1-ATPase, with no adjustable parameters, when corrections are made for the differences in the nucleotide species in the experiments, even though the occupancy in the ATPase in the controlled rotation experiment is at most one whereas that in the stalling experiment is two or three?

v) Can a structural elasticity of the ATPase be extracted from the equilibrium constant vs. rotor angle data for various nucleotides?

Results

Elastic Chemomechanical Group Transfer Theory. In our previous study (16) the binding and release of nucleotides were treated in F_1-ATPase based on a formalism originally proposed for electron transfers (17) and adapted to other transfers (18), including proton (19) and methyl cation (20) transfers. In the theory a thermodynamic driving force that determines the rate and equilibrium constants in the experiments for any reaction step, including nucleotide binding, is the change in the relevant Gibbs free energy of reaction for that step. A thermodynamic cycle (Scheme 1) (16) provides a basis for relating the free energies of a change accompanying nucleotide binding in free rotation, ΔG_0^0 (Fig. S1), to the binding free energy $\Delta G^0(\theta)$ at a constant rotor angle θ. In the present treatment we consider a quasistatic approximately constant θ in any observation interval—quasistatic because the rotor shaft is rotated slowly during the controlled rotation.

$$\begin{array}{ccc} & \Delta G^0(\theta) & \\ G_r^0(\theta) & \rightarrow & G_p^0(\theta) \\ w^r \uparrow & & \downarrow -w^p \\ G_r^0(\theta_i) & \rightarrow & G_p^0(\theta_f) \\ & \Delta G_0^0 & \end{array}$$

Scheme 1.

In Scheme 1, $G_r^0(\theta)$ and $G_p^0(\theta)$ denote the free energies of the system in its "reactant" and "product" states (unbound and bound ATP states in the present θ range) when the magnetic tweezers hold the rotor at an angle θ. The system is relaxed at the initial and final dwell angles $\theta_i = 0°$ and $\theta_f = 80°$. As before (16), it is assumed that rotary motors exhibit a harmonic response to twisting torques described by an effective stiffness κ (15, 21, 22), and so in Scheme 1 we recall from ref. 16 that $w^r = \kappa/2(\theta - \theta_i)^2$ and $w^p = \kappa/2(\theta - \theta_f)^2$. For the θ-dependent $k_f(\theta)$ and $k_b(\theta)$ in Eqs. **3** and **4** given later a quadratic group transfer theory relation is used. This relation, given in ref. 16 as equation 10, relates $\Delta G^0(\theta)$ in Scheme 1 and the free energy barrier $\Delta G^\dagger(\theta)$ that the nucleotide needs to overcome during binding when it transfers from solution into the pocket (16–18).

Application of the Theory to Cy3-Nucleotides. In the analysis (16) of the stalling experiments linear ln k_f, ln k_b, and ln K vs. θ were predicted for the θ range treated experimentally. Given the similarities between the probed binding/release processes and the exponential-like rate vs. rotor data in the controlled rotation experiments (Fig. S2) compared to those in stalling experiments, in the present article we apply the chemomechanical group transfer theory (16) to the processes of nucleotide binding and release in controlled rotation experiments. In the present treatment we consider a quasistatic approximately constant rotor angle in any observation interval j of duration t on Fig. S3—quasistatic because the rotor shaft is rotated slowly during the controlled rotation. Although controlled rotation experiments provide binding and release events over nearly the complete 360° range (4), in the present article we compare the experimental results with the theoretical predictions in the angular range of (−50°, 50°), where the current stalling and controlled rotation experiments overlap. We note that according to the notation adopted in single-molecule experiments (1, 4, 14), $\theta = 0°$ is set at the ATP binding dwell.

For Cy3-ATP available data from the stalling and other experiments are used to predict the absolute values for the $k_f(\theta)$, $k_b(\theta)$, and $K(\theta)$ in the controlled rotation experiments, including therefore the slopes ($\partial \ln k_f/\partial\theta$ and $\partial \ln k_b/\partial\theta$) and the values at $\theta = 0$, $\ln k_f(0)$ and $\ln k_b(0)$ [and hence $\ln K(0)$]. The θ-dependent rate and equilibrium constants are determined, as discussed below, by the following quantities: the relevant torsional stiffness of the structure κ, the change of the locally stable rotor angle during rotation $\theta_f - \theta_i$, the "reorganization energy" λ, the Brønsted slope at $\theta = 0$, $\alpha(0)$, and the binding and release rate constants for Cy3-ATP at $\theta = 0$, $k_f(0)$, and $k_b(0)$. The procedure to use the theory together with prior independent experimental data first involves deducing functional forms for $k_f(\theta)$, $k_b(\theta)$, and $K(\theta)$, then providing the values of the quantities that appear in their expression, as follows.

For the $K(\theta)$, from equation 5 of ref. 16 it follows that

$$kT\ln K(\theta)=kT\ln K(0)+\theta\,\kappa(\theta_f-\theta_i). \quad [1]$$

To calculate the $k_f(\theta)$, we first introduce the value of the Brønsted slope $\alpha(\theta)=\partial\ln k_f(\theta)/\partial\ln K(\theta)$ (18, 23, 24), at the angle $\theta=0$,

$$\alpha(0)=\left[\partial\ln k_f(\theta)/\partial\ln K(\theta)\right]\big|_{\theta=0}. \quad [2]$$

From our previous treatment (16), $k_f(\theta)$ as a function of θ is given by

$$kT\ln k_f(\theta)=kT\ln k_f(0)+\theta\alpha(0)\kappa(\theta_f-\theta_i)-\theta^2\kappa^2(\theta_f-\theta_i)^2\Big/4\lambda. \quad [3]$$

For the release of the nucleotide, $k_b(\theta)=k_f(\theta)/K(\theta)$, and so from Eqs. **1**–**3**,

$$kT\ln k_b(\theta)=kT\ln k_b(0)-\theta[1-\alpha(0)]\kappa(\theta_f-\theta_i)-\theta^2\kappa^2(\theta_f-\theta_i)^2\Big/4\lambda. \quad [4]$$

We consider next the effect of changing from the wild-type nucleotide ATP to fluorescent species Cy3-ATP, as well as the condition of single-site occupancy. If κ describes the effective stiffness of rotor, the β lever arm, and to some extent the bonding network with the nucleotide, we can presume that it is not significantly affected by changing the substrate to Cy3-nucleotide, because the Cy3 part remains outside the pocket because of the linker, as discussed in a following section.

Next, we describe a procedure to provide the values for the quantities $\theta_f-\theta_i$, κ, λ, $\alpha(0)$, $k_f(0)$, and $k_b(0)$, also listed in Table 1, which appear in Eqs. **1**, **3**, and **4** and are used to construct the theoretical plot. A part of the procedure given below relies on a procedure described previously in ref. 16.

i) Based on the previous description, we use the $\kappa=16$ pN·nm/rad^2 found earlier (16) from the stalling experiments.

ii) The angular changes of 80° and 40° in the stepping rotation have been reported to remain unchanged when ATP is replaced by Cy3-ATP in free rotation experiments (1), so we continue to use $\theta_f-\theta_i=80^o$.

iii) The reorganization energy λ appears explicitly in the quadratic term in Eqs. **3** and **4**, and for its value we use $\lambda=68$ kcal/mol. It was calculated in equation 18 of ref. 16 for the stalling experiments using a work (W^r) and two free energy ($\Delta G_0^{\dagger}$ and ΔG_0^0) terms provided in table 3 of ref. 16.* A simpler procedure based on the method given in ref. 16 to estimate these three quantities is described in *Supporting Information*, Fig. S1.

iv) For the Brønsted slope, an $\alpha^{\mathrm{Cy3-ATP}}(0)\cong 0.5$ (Table 1) can be inferred for Cy3-ATP binding from the $\alpha^{\mathrm{ATP}}(0)=0.48\cong 0.5$, calculated in our previous treatment of stalling experiments using equation 12 of ref. 16 with the same W^r, $\Delta G_0^{\dagger}$, and ΔG_0^0 terms given in *Supporting Information*, and the quantities from steps *i* and *ii* above.

*Correction for ref. 16: on page 4, column 2 "$\Delta G_0^{\dagger}-W^r=14.1$ kcal/mol" should read "$\Delta G_0^{\dagger}-W^r=11.3$ kcal/mol." This change causes the two λ values in table 3 and table 4, "56" and "55," to be changed to "68" and "67," respectively. Because α for ATP and GTP binding is close to 1/2, $\Delta G_0^0\ll 2\lambda$, according to equation 12. α is relatively insensitive to changes in a quadratic term $\Delta G^0/4\lambda$ that has a small contribution to the deviation of α from 0.5. The new α for ATP binding, 0.476, rounds off to "0.48" instead of "0.47" in table 3. All other numbers involving the comparison of theory and experiment remain unchanged, and so no conclusions are affected.

Table 1. Summary of effective quantities and comparison between theoretical predictions and experiment on the angle-dependent rate constants for Cy3-ATP binding

Properties used in theory*			Controlled rotation, rates vs. θ		
Quantity	Value*	Source†	Quantity	Theory‡	Experiment†
$\theta_f-\theta_i$	80°	F (1)	$k_f(0)$	0.9	~1.2
λ	68	EFS (16)	$d\ln k_f/d\theta$	0.49	~0.48
κ	16	S (3, 16)	$k_b(0)$	1.3	~1.0
$\alpha(0)$	0.5	EFS (16)	$d\ln k_b/d\theta$	−0.49	~−0.48
$k_f^{\mathrm{ATP}}(0)$	9.2	S (3)			
$k_b^{\mathrm{ATP}}(0)$	0.13	S (3)			
$k_{f,0}^{\mathrm{Cy3-ATP}}/k_{f,0}^{\mathrm{ATP}}$	0.1	E (25)/F (1)			
All of the above. EFS (1, 3, 4, 16, 25)			k_f^{rep}, k_b^{rep}, and K^{rep}; Fig. S4*A*		
All of the above. EFS (1, 3, 4, 16, 25)			Actual k_f, k_b, and K; Fig. 2		

*k_f and k_b are in units of (micromoles seconds)$^{-1}$ and seconds^{-1}, respectively; $d\ln k_f/d\theta$ and $d\ln k_b/d\theta$ are in 1/10°; κ is in piconewtons·nanometer/rad^2; and λ is in kilocalories per mole.

†Properties were extracted from single-molecule [free rotation (F) and stalling (S)] and ensemble (E) experiments.

‡The values in this column are approximate.

v) Changing from ATP to Cy3-ATP changes the $kT\ln k_f(0)$ term. To calculate $k_f(0)$, we first note that theory (16) relates it to the binding rate constant in free (unconstrained) rotation $k_{f,0}$ by a relation deduced from equations 5–9 of ref. 16, $kT\ln k_f(0)=kT\ln k_{f,0}-\alpha(0)\kappa(\theta_f^2-\theta_i^2)/2+(\theta_i+\theta_f)^2\kappa^2(\theta_f-\theta_i)^2/\ 16\lambda$. Because, according to steps *i*–*iv*, the last two terms are unchanged if ATP is changed to Cy3-ATP, the ratio of $k_f(0)/k_{f,0}$ will not change either, and so

$$k_{f,0}^{\mathrm{Cy3-ATP}}\Big/k_{f,0}^{\mathrm{ATP}}=k_f^{\mathrm{Cy3-ATP}}(0)\Big/k_f^{\mathrm{ATP}}(0). \quad [5]$$

From stalling experiments (3), $k_f^{\mathrm{ATP}}(0)=9.2\cdot 10^6\ \mathrm{M}^{-1}\,\mathrm{s}^{-1}$, the experimentally (1) measured ratio of $k_f^{\mathrm{ATP}}/k_f^{\mathrm{Cy3-ATP}}\cong 10$, reported in Table 1, yields $k_f^{\mathrm{Cy3-ATP}}(0)=0.9\cdot 10^6\ \mathrm{M}^{-1}\cdot\mathrm{s}^{-1}$.

vi) To provide a value for $k_b(0)$ that appears in Eq. **4**, we note that for the $\alpha(0)\cong 0.5$ a suppression by some factor in the forward binding rate corresponds to an enhancement by the same factor in the backward rate. In particular, because from ref. 3 $k_b^{\mathrm{ATP}}(0)=0.13\ \mathrm{s}^{-1}$, we calculate $k_b^{\mathrm{Cy3-ATP}}(0)=1.3\ \mathrm{s}^{-1}$. Finally, from Eq. **1** and steps *iv* and *v* we deduce $K(0)=k_f(0)/k_b(0)=0.7\times 10^6\ \mathrm{M}^{-1}$.

For Cy3-ADP, the controlled rotation data were simply fitted to the functional form given in Eqs. **1**–**4** by assuming the same $\theta_f-\theta_i=80°$ and $\lambda=68$ kcal/mol, and adjusting the other parameters, because there were no data to predict the Cy3-ADP values from prior experiments.

Rate Constant Estimate in Experiments and Missed Events. In the present analysis, we treat the controlled rotation data of Adachi et al. (4) and use some of the procedure devised by these authors in their analysis, as follows. When a site is occupied, the nucleotide fluoresces; otherwise, fluorescence drops to a background level, giving rise to site-occupancy trajectories along which σ switches between 0 and 1. The binding and release events along the trajectories were assigned to specific sites and grouped into 36 consecutive intervals of $\Delta\theta=10°$, with a rotation time $t=0.14$ s per interval, during which the binding and release rates were considered as approximately constant. Within each $\Delta\theta$ simple two-state kinetics was assumed with angle-dependent binding and release rate constants. The forward rates can be estimated as the number of $0\rightarrow 1$ events divided by time T_0 spent in the $\sigma=0$

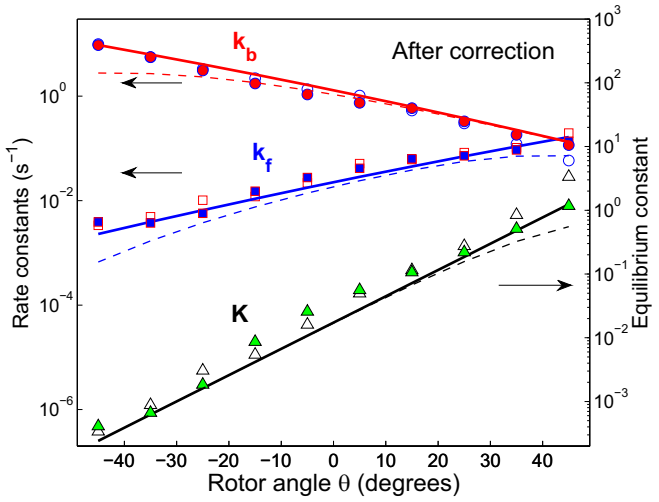

Fig. 2. Corrected binding and release rate and equilibrium rate constants vs. θ angle for Cy3-ATP in the presence (solid squares, circles, and triangles) and absence of P_i (open symbols) in solution. The experimental data of Adachi et al. (4), corrected for missed events and an error due to replacing T_0 by T, are compared with their theoretical counterparts (solid lines). Dashed lines show the data without corrections.

state in the trajectory. Adachi et al. (4) replaced T_0 with the total time T, because the system presumably spends relatively little time in the $\sigma = 1$ state at all rotor angles. The backward rates were estimated as the number of $1 \rightarrow 0$ events divided by the time T_1. The reported rate constants, reproduced in Fig. S2, are seen to have an exponential-like dependence on the rotor angle, and so can quickly become very high. Some binding events will then be missed due to the limited time resolution of the single-molecule fluorescence used to monitor these events. As a result, the experimentally estimated rate constants will be in some error if left uncorrected. In particular, the times spent in the $\sigma = 1$ state shorter than $3\tau = 0.1$ s were neglected in the analysis (4), where τ denotes the image frame acquisition time in the experimental procedure (3τ in order that the fluorescent state lasts for more than a mere fluctuation seen in one frame). We take into account the effect of both the t and τ timescales which can, to some extent, bias the outcome, a common feature in single-molecule spectroscopy (26). The methods we used to make corrections due to the missed events and using T instead of T_0 are outlined in *Materials and Methods* and further details are given in *Supporting Information*.

Predictions and Comparison with Experiment. Using the theory, the kinetic and thermodynamic properties for the controlled rotation are predicted in Fig. 2, independently of the controlled rotation (25) experiments, from available experimental data. The data used for the predictions, summarized in Table 1, are from previous stalling (3), free rotation (1, 22), and ensemble biochemical (25) experiments.

The theoretically predicted rates are plotted in Fig. 2 as solid lines. A single set of theoretical $k_f(\theta)$, $k_b(\theta)$, and $K(\theta)$ curves are compared with two experimental datasets on Cy3-ATP binding, because the presence or absence of solution P_i does not yield statistically distinguishable rates (Fig. S2). From the predicted rate constants the corrections were calculated. These theoretical corrections, including the terms for both the missed events and replacing T with T_0 in the reported experimental estimate for the forward rate constant, were applied to correct the original experimental data from Fig. S2 and to produce the corrected experimental $k_f(\theta)$, $k_b(\theta)$, and $K(\theta)$ results with which theory was then compared in Fig. 2. (In an alternative way of comparing experiment and theory, the theoretical counterparts of the reported rate constants were also calculated from the theory and are compared in Fig. S4 with the unmodified experimental values from Fig. S2.)

For the ADP counterpart of Cy3-ATP, Cy3-ADP, there are presently no experimental data available for independent prediction of the controlled rotation experiments. Accordingly, we simply extract from the experimental rate constants for Cy3-ADP in Fig. 3 the properties relevant for the binding and release of Cy3-ADP, by fitting the experimental data with theory-based plots (*Materials and Methods*). One deduced constant for the Cy3-ADP from the $\ln K$ vs. θ plot, using Eq. **1**, is the spring constant, $\kappa^{\mathrm{Cy3-ADP}} = 12$ pN·nm/rad^2. It is smaller by 25% than the spring constant for Cy3-ATP (and ATP) binding $\kappa^{\mathrm{Cy3-ATP}} =$ 16 pN·nm/rad^2. The $k_f(0)$ for Cy3-ADP binding was also found to be smaller than that of Cy3-ATP binding by a factor of ~2. For the other quantities, $\alpha(0)$ and $k_b(0)$, the fitting procedure yielded values indistinguishable from those for Cy3-ATP. A comparison of the experimental k^{rep}, k_b^{rep}, and K^{rep} with the theoretical fits to the curves is given in Fig. S5.

Discussion

The theoretical predictions for Cy3-ATP binding and release given in Fig. 2 and Fig. S4 and Table 1 are seen to compare well with their experimental counterparts, both in the presence and absence of P_i in solution. The corrected experimental data are compared with the theoretical values and show the exponential dependence predicted by theory. The $\ln k_f$ and $\ln k_b$ over the range investigated are now almost linear in θ, and within the present treatment $\ln K$ is exactly linear in θ. This dependence was also seen in the stalling experiments. The agreement in Fig. 2, with no adjustable parameters, illustrates the applicability of the group transfer theory to the system for the various nucleotide species. In particular, single-molecule rate data involving the binding of ATP and GTP, the slope of $\ln k_f(\theta)$, $\ln k_b(\theta)$ and so $\ln K(\theta)$ vs. θ, were predicted in the stalling experiments and agreed well with results (with the larger scatter for the GTP) (16); in that work there were no independent data to predict the absolute value of the rate constants. Now, for Cy3-ATP, both in the presence and absence of solution P_i, the absolute values of these quantities are predicted for the controlled rotation experiments. As noted earlier the rate constants for Cy3-ADP

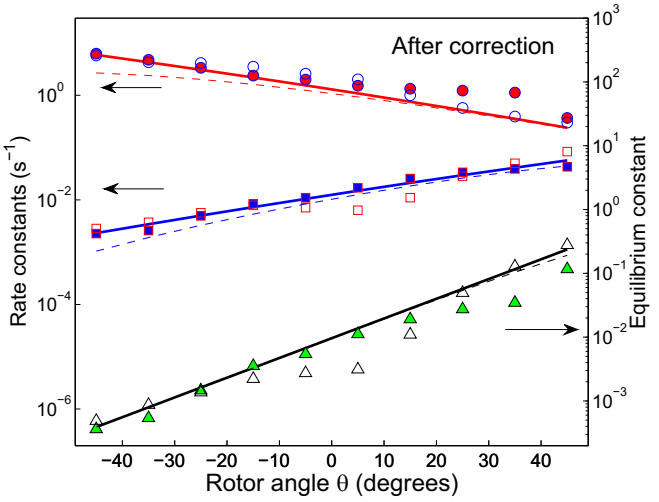

Fig. 3. Corrected binding and release rate constants and equilibrium rate constants for Cy3-ADP in the presence and absence of P_i in solution. The theoretical $\ln K^{\mathrm{rep}}$ vs. θ was fitted to experiment, which yielded $\kappa^{\mathrm{ADP}} = 12$ pN·nm/rad^2 and $k_f^{\mathrm{ADP}}(0) = 4.6 \times 10^6$ M^{-1}·s^{-1} $= 0.5 \cdot k_f^{\mathrm{ATP}}(0)$. The notations from Fig. 2 apply here (ATP is replaced by ADP) (e.g., the dashed lines denote the uncorrected data).

binding and release are seen to be unaffected, within the data scatter, by whether or not P_i is present in solution.

When extending the treatment to the Cy3-ATP species the changes affected their absolute value but did not affect the $\ln K$ vs. θ slope. In particular, neither the step size $\theta_f - \theta_i = 80°$ nor, as seen in the prediction of the theoretical curves in Fig. 2 and Fig. S4, the stiffness κ was altered by the Cy3 moiety attached to the nucleotide. Therefore, in Eq. **1**, when the equilibrium constant $K(\theta)$ is changed by replacing ATP with Cy3-ATP, the change does not affect the slope $\partial \ln K/\partial\theta$, because the latter depends on $\kappa(\theta_f - \theta_i)$. Similarly, in Eqs. **3** and **4** it can be seen that by replacing ATP with Cy3-ATP the change does not affect the slopes $\partial \ln k_f/\partial\theta$ and $\partial \ln k_b/\partial\theta$. We note that of the six quantities, $\theta_f - \theta_i$, κ, λ, $\alpha(0)$, $k_f(0)$, and $k_b(0)$, used to predict the controlled rotation data on Cy3-ATP, only five are independent. Because currently there are no experimental data to estimate $k_b(0)$, we first estimated $\alpha(0)$, then used its value to estimate $k_b(0)$. Alternatively, stalling experiments with Cy3-ATP could provide a $k_b(0)$ value, and so $\alpha(0)$ could be calculated, as an "auxiliary" quantity from the other five.

The theory, in this application to treat another nucleotide species, Cy3-ADP, is seen in Fig. 3 to fit the rate vs. rotor angle θ data from controlled rotation experiments. There is no prediction of the k_f and k_b because free rotation or stalling experiments do not provide data on ADP binding in the region of interest ($-50° < \theta < 50°$) or indeed for any range of θ. The results from Figs. 2 and 3 show that the chemomechanical group transfer theory can be used for treating the binding and release rates of various nucleotides. Again, any differences due to introducing P_i in the solution are seen in Figs. 2 and 3 and Fig. S2 to be too small to be detectable by the current experimental resolution. A difference in the values of $\ln k_f$ and $\ln k_b$ vs. rotor angle for the binding of fluorescent ATP and ADP is seen in the experiments in Figs. 2 and 3 and Fig. S2 and Table 1. In particular, there is a difference in the slope of the $\ln K(\theta)$ vs. θ dependence, and so a difference in the effective torsional spring constant κ (16 vs. 12 $pN \cdot nm/rad^2$) becomes apparent. Within the framework of the theory it points to a difference between the stiffness of the structure in the presence of various nucleotides. Adding the fluorescent group Cy3 to ATP did not affect the κ, as judged by the agreement of predictions and experiment for κ, and so the difference in their interactions did not affect the spring constant, but the interactions are affected by replacing the ATP group by ADP.

In free rotation Cy3-ATP binds about 10 times slower than ATP (1), an observation that we have incorporated into the present analysis. Two differences between stalling and controlled rotation experiments that can affect the k_f are the total site occupancy and the nature of the binding nucleotide species. Stalling experiments revealed that the k_f of ATP in the vicinity of $\theta = 0°$ is independent of the presence or absence of ADP in the counterclockwise neighbor subunit (3). This observation is corroborated by measurements of the bimolecular rate constant for ATP binding; in free rotation it is independent of the ATP concentration in the nanomolar to millimolar range (27), whereas the average site occupancy in the ATPase varies from 1 to 3 (28). Accordingly, the k_f of ATP at 0° to an all empty enzyme is indistinguishable from that of binding when one or more nucleotides are occupying the other subunits. It follows that any difference in the k_f and k_b in stalling and controlled rotation experiments is not due to the difference in site occupancy but rather to the difference between the nucleotide species. Consistent with this result is that when the k_f for the controlled rotation experiment (unisite occupancy) is predicted from free rotation rates (bisite occupancy), the agreement is seen in Fig. 2 and Fig. S4 to be very good.

The effect of missed events and the use of T_0 instead of T for the reported $\ln k_f$ s is to always "curve down" (make concave) the $\ln k_f$ and $\ln k_b$ vs. θ plots. After correcting for these effects, these functions show now only a small residual curvature, as depicted in Figs. 2 and 3 by comparing the reported (dashed lines) and the corrected data. The statistics of missed events and the difference between T and T_0 depend on the values k_f and k_b, and hence, through the binding rate, the concentration. In Figs. 2 and 3, we plot the pseudounimolecular k_f (units of $seconds^{-1}$) rather than the bimolecular rate constant, thus providing the relevant timescale. The number of missed $0 \to 1 \to 0$ events is appreciable at low θ values, that is, at $\theta \sim -50°$, when k_b becomes large compared with $1/t$ and much larger than k_f, resulting in significant corrections for both k_f and k_b, as seen in Fig. 2. Meanwhile, the error introduced in the k_f by using T_0 instead of T becomes significant when θ approaches 50°, where k_f becomes comparable to or larger than k_b, and the reported forward rate constant is seen to be increasingly lower than the actual k_f. Indeed, most of the correction at $\theta = 50°$ is due to replacing T_0 with T, rather than to missed events.

The present analysis suggests that the effective stiffness κ of the structure is determined largely by the structure of the rotor (and the β subunit lever arm), and to a smaller extent (e.g., 16 vs. 12 $pN \cdot nm/rad^2$) by the interaction of the β subunit with the binding nucleotide. This difference between the $\ln K$ vs. θ slope of Cy3-ATP and Cy3-ADP structures, and hence in κ, was found both in the presence and absence of P_i in the solution. Meanwhile, it can be inferred from the agreement of theory and experiment that κ is insensitive to adding a fluorescent moiety to the ATP nucleotide species.

These findings are consistent with a picture in which the fluorescent Cy3 moiety remains outside of the β subunit, whereas the nucleotide enters the pocket during binding. This is structurally possible, because the two are linked by a flexible tether (29) that can stretch to ~1.5 nm. Being outside of the subunit the Cy3 does not interfere with the network of hydrogen and other bonds in the pocket, involving the nucleotide and the host β subunit, and so it does not affect the relevant κ. Meanwhile, the tether is presumably stretched out when the nucleotide is in the pocket and so may limit the degrees of freedom: The tethered Cy3 moiety has more "freedom" in the solution than when bound to the outside of the ATPase and so shifts the equilibrium constant K toward the unbound state.

The spring constant of 16 $pN \cdot nm/rad^2$ is a little smaller than the 20 $pN \cdot nm/rad^2$ measured by Junge and coworkers (22). Their measurement may include additional parts of the rotor–stator complex. The κ obtained from a $\ln K$ vs. θ plot in the stalling experiment is intrinsically consistent with its present use to predict the κ for the controlled rotation experiment, because it refers to the same process.

One can ask whether the two-state kinetics assumed in the analysis of binding/release events in the $\Delta\theta$ intervals can be validated. We note that in the stalling experiments the distribution of forward/backward steps upon release were verified to be single exponential and so to follow two-state kinetics. Although in the controlled rotation experiments such a test is not feasible due to the limited amount of data, the two-state kinetics is nevertheless found to be valid, because the θ-dependent k_f and k_b are consistent with those in stalling experiments (and with our theory), and so there are no hidden states detectable on the experimental timescales.

The connection between binding and release events to the rotation of the γ shaft has been investigated by several groups using structural calculations (30–35). A question arising from our study that simulations could treat is the evolution of the hydrogen-bonding network during structural displacements of a β subunit, and how it is affected by the presence of the binding nucleotide. The hydrogen-bond "order" can serve as a collective reaction coordinate (16, 18) for the binding transition of the nucleotide. The Brønsted slope identifies the nature of the transition state (16, 18) and it was recently applied to treat the gating charge fluctuations in membrane proteins as a quantity

related to charge transport (36). In that study the gating voltage is a control parameter analogous to the θ of the F_1-ATPase in our treatment.

Conclusions

The elastochemical theory of the rotary biomolecular motors described here provides an interpretation and treatment for the controlled rotation experiments on the F_1-ATPase enzyme. For these experiments the theory makes and tests predictions using independent experimental data on binding and release of fluorescent ATP given in Table 1 and Fig. 2, in the range of rotor angles θ where the controlled rotation and stalling experiments overlap. The dependence of the rate and equilibrium constants on θ from the theory are compared with experiment and are found to be in agreement. The theoretical model originally proposed to treat nucleotide binding and release in stalling experiments was found to be applicable to controlled rotation experiments on fluorescent ATP and ADP analogs, even though there is a marked difference in conditions—single vs. multiple site occupancy. By taking into account the effect of missed events in the experiments and the error due to using T instead of T_0, the specific nature of the $\log k_f$ and $\log k_b$ vs. θ data was explained. It was found that the effective torsional spring constant is smaller for binding of ADP than of ATP, but it is not affected by the presence of the fluorescent Cy3 moiety in Cy3-ATP and Cy3-ADP. The effect of the Cy3 tethered to the nucleotide was found, not surprisingly, to shift the equilibrium constant for binding toward release by limiting the degrees of freedom of the nucleotide in the binding pocket. In the Introduction several question were posed. In each case, the answers are seen to be affirmative. The controlled rotation experiments also provide binding and release rate data over much of the 360° range of θ. Furthermore, one may anticipate that the present elastic group transfer theory applies to relatively small, compact domain motions and not to large changes such as folding of proteins.

Materials and Methods

Correction of Controlled Rotation Data. The theoretical counterparts of the reported k_f^{rep} and k_b^{rep} (Eqs. S1 and S2) are calculated, from the averaged values over an interval j, using the actual k_f and k_b predicted by theory (Cy3-ATP) or as fitting functions (Cy3-ADP). Then, the corrections are calculated as the differences $k_f - k_f^{\text{rep}}$ and $k_f - k_f^{\text{rep}}$. In these calculations the terms due to the missed events are evaluated. Because the denominator of k_f^{rep} (Eq. S2) T is used, the error due to replacing T_0 with T is explicitly taken into account (*Supporting Information*).

Fitting Procedure for Cy3-ADP. We assumed $\theta_f - \theta_i = 80°$. The search for a "best fit" then involved finding a pair of $k_f(\theta)$ and $k_b(\theta)$ that remain within the scatter of the experimental data for all θ. These experimental data in Fig. 3 originated from correcting the reported data by calculating the missed events and the change due to using T instead of T_0.

ACKNOWLEDGMENTS. We thank Drs. Imre Derényi and Kengo Adachi for helpful discussions and comments and the reviewers for useful suggestions. This work was supported by the Office of the Naval Research, the Army Research Office, and the James W. Glanville Foundation.

1. Adachi K, et al. (2007) Coupling of rotation and catalysis in F(1)-ATPase revealed by single-molecule imaging and manipulation. *Cell* 130(2):309–321.
2. Spetzler D, et al. (2009) Single molecule measurements of F1-ATPase reveal an interdependence between the power stroke and the dwell duration. *Biochemistry* 48(33):7979–7985.
3. Watanabe R, et al. (2011) Mechanical modulation of catalytic power on F1-ATPase. *Nat Chem Biol* 8(1):86–92.
4. Adachi K, Oiwa K, Yoshida M, Nishizaka T, Kinosita K, Jr (2012) Controlled rotation of the F_1-ATPase reveals differential and continuous binding changes for ATP synthesis. *Nat Commun* 3:1022.
5. Yasuda R, Noji H, Yoshida M, Kinosita K, Jr, Itoh H (2001) Resolution of distinct rotational substeps by submillisecond kinetic analysis of F1-ATPase. *Nature* 410(6831):898–904.
6. Nishizaka T, et al. (2004) Chemomechanical coupling in F1-ATPase revealed by simultaneous observation of nucleotide kinetics and rotation. *Nat Struct Mol Biol* 11(2):142–148.
7. Senior AE (2007) ATP synthase: Motoring to the finish line. *Cell* 130(2):220–221.
8. Braig K, Menz RI, Montgomery MG, Leslie AG, Walker JE (2000) Structure of bovine mitochondrial F(1)-ATPase inhibited by Mg(2+) ADP and aluminium fluoride. *Structure* 8(6):567–573.
9. Boyer PD (1993) The binding change mechanism for ATP synthase–Some probabilities and possibilities. *Biochim Biophys Acta* 1140(3):215–250.
10. Junge W, Sielaff H, Engelbrecht S (2009) Torque generation and elastic power transmission in the rotary F(O)F(1)-ATPase. *Nature* 459(7245):364–370.
11. Weber J (2010) Structural biology: Toward the ATP synthase mechanism. *Nat Chem Biol* 6(11):794–795.
12. Walker JE (2013) The ATP synthase: The understood, the uncertain and the unknown. *Biochem Soc Trans* 41(1):1–16.
13. Watanabe R, Noji H (2013) Chemomechanical coupling mechanism of F(1)-ATPase: Catalysis and torque generation. *FEBS Lett* 587(8):1030–1035.
14. Watanabe R, Noji H (2014) Timing of inorganic phosphate release modulates the catalytic activity of ATP-driven rotary motor protein. *Nat Commun* 5:3486.
15. Watanabe R, Iino R, Noji H (2010) Phosphate release in F1-ATPase catalytic cycle follows ADP release. *Nat Chem Biol* 6(11):814–820.
16. Volkán-Kacsó S, Marcus RA (2015) Theory for rates, equilibrium constants, and Brønsted slopes in F1-ATPase single molecule imaging experiments. *Proc Natl Acad Sci USA* 112(46):14230–14235.
17. Marcus RA, Sutin N (1985) Electron transfers in chemistry and biology. *Biochim Biophys Acta* 811:265–322.
18. Marcus RA (1968) Theoretical relations among rate constants, barriers, and brønted slopes of chemical reactions. *J Phys Chem* 72(3):891–899.
19. Roston D, Islam Z, Kohen A (2014) Kinetic isotope effects as a probe of hydrogen transfers to and from common enzymatic cofactors. *Arch Biochem Biophys* 544:96–104.
20. Lewis ES, Hu DD (1984) Methyl transfers. *J Am Chem Soc* 106:3294–3296.
21. Pänke O, Cherepanov DA, Gumbiowski K, Engelbrecht S, Junge W (2001) Viscoelastic dynamics of actin filaments coupled to rotary F-ATPase: Angular torque profile of the enzyme. *Biophys J* 81(3):1220–1233.
22. Wächter A, et al. (2011) Two rotary motors in F-ATP synthase are elastically coupled by a flexible rotor and a stiff stator stalk. *Proc Natl Acad Sci USA* 108(10):3924–3929.
23. Szabo A (1978) Kinetics of hemoglobin and transition state theory. *Proc Natl Acad Sci USA* 75(5):2108–2111.
24. Schweins T, Warshel A (1996) Mechanistic analysis of the observed linear free energy relationships in p21ras and related systems. *Biochemistry* 35(45):14232–14243.
25. Weber J, Senior AE (1997) Catalytic mechanism of F1-ATPase. *Biochim Biophys Acta* 1319(1):19–58.
26. Volkán-Kacsó S (2014) Two-state theory of binned photon statistics for a large class of waiting time distributions and its application to quantum dot blinking. *J Chem Phys* 140(22):224110.
27. Sakaki N, et al. (2005) One rotary mechanism for F1-ATPase over ATP concentrations from millimolar down to nanomolar. *Biophys J* 88(3):2047–2056.
28. Shimo-Kon R, et al. (2010) Chemo-mechanical coupling in F(1)-ATPase revealed by catalytic site occupancy during catalysis. *Biophys J* 98(7):1227–1236.
29. Oiwa K, et al. (2003) The 2′-O- and 3′-O-Cy3-EDA-ATP(ADP) complexes with myosin subfragment-1 are spectroscopically distinct. *Biophys J* 84(1):634–642.
30. Mukherjee S, Warshel A (2011) Electrostatic origin of the mechanochemical rotary mechanism and the catalytic dwell of F1-ATPase. *Proc Natl Acad Sci USA* 108(51):20550–20555.
31. Hayashi S, et al. (2012) Molecular mechanism of ATP hydrolysis in F1-ATPase revealed by molecular simulations and single-molecule observations. *J Am Chem Soc* 134(20):8447–8454.
32. Okazaki K, Hummer G (2013) Phosphate release coupled to rotary motion of F1-ATPase. *Proc Natl Acad Sci USA* 110(41):16468–16473.
33. Mukherjee S, Warshel A (2015) Dissecting the role of the γ-subunit in the rotary-chemical coupling and torque generation of F1-ATPase. *Proc Natl Acad Sci USA* 112(9):2746–2751.
34. Mukherjee S, Warshel A (2015) Brønsted slopes based on single-molecule imaging data help to unveil the chemically coupled rotation in F1-ATPase. *Proc Natl Acad Sci USA* 112(46):14121–14122.
35. Sugawa M, et al. (2015) F1-ATPase conformational cycle from simultaneous single-molecule fret and rotation measurements. *Proc Natl Acad Sci USA* 113(21):E2916–E2924.
36. Kim I, Warshel A (2016) A microscopic capacitor model of voltage coupling in membrane proteins: Gating charge fluctuations in ci-vsd. *J Phys Chem B* 120(3):418–432.
37. MathWorks (2014) MATLAB. The language of technical computing (version R2014b) (MathWorks, Inc., Natick, MA).

Supporting Information

Volkán-Kacsó and Marcus 10.1073/pnas.1611601113

Estimation of λ and $\alpha(0)$

Here we provide a summary of the procedure described in ref. 16 to calculate λ and $\alpha(0)$ from available free rotation, stalling, and ensemble biochemical experimental data. In equation 12 of ref. 16 $\alpha(0)$ [i.e., $\alpha(\theta)$ at $\theta=0$], and in equation 18 λ is given as a function of three energy quantities, shown in bold in the energy diagram in Fig. S1: the work term for the weak binding in the reactant (R) state, W^r, the free energy barrier in the collision-based theory of binding, $\Delta G_0^{\dagger}$, and the standard free energy of reaction defined relative to the R state, ΔG_0^0. These quantities involved in the binding of ATP are defined relative to the states given in Fig. S1, a state (S) in which the ATP molecule is found in the solution, a reactant state (R), which involves the weak binding of ATP at the entrance site, the transition state (TS), and a product state (P) in which the ATP occupies the binding pocket. We now summarize the procedure to estimate the value of the three quantities, also given in Fig. S1.

i) The W^r is estimated to be −9.1 kcal/mol for ATP binding, calculated from the binding affinity of −6.3 kcal/mol to the empty open-conformation subunit [from a dissociation constant (25) of 25 μM] minus an entropic contribution to the free energy change $kT\ln kT/hZ=2.8$ kcal/mol.

ii) A $\Delta G_0^{\dagger}=5.0$ kcal/mol estimate is yielded by collision theory, assuming a collision frequency of $Z=10^{11}$ $M^{-1}\cdot s^{-1}$. The free rotation rate constant for ATP binding is $k_{f0}=2\times10^7$ $M^{-1}\cdot s^{-1}$ (1), which is used in equation 8 of ref. 16 to give the above estimate for $\Delta G_0^{\dagger}$.

iii) The $\Delta G_0^0=-6.0$ kcal/mol estimate for ATP binding can be calculated, according to Fig. S1, by subtracting the binding affinity of −6.3 kcal/mol for the R state from the standard free energy of reaction defined relative to the solution state (S), $\Delta G_{s0}^0=-kT\ln K_0=-12.3$ kcal/mol (3). This method, based on Fig. S1 for evaluating ΔG_0^0, is simpler than that used in ref. 16.

Correcting the Reported Controlled Rotation Data

Here we describe a theoretical method to calculate corrections for the data reported by Adachi et al. (4) due to the effects of (*i*) missed events and (*ii*) replacing T_0 with T.

If θ_j is the rotor angle at the center of the j^{th} interval, then, according to Adachi et al. (4), we use for the reported ("rep") rate constant estimates in the 36 intervals the values used in their analysis,

$$k_f^{\text{rep}}(\theta_j)=N(0\to1,j)/T, \qquad \text{[S1]}$$

$$k_b^{\text{rep}}(\theta_j)=N(1\to0,j)/T_1(j), \qquad \text{[S2]}$$

where $N(0\to1,j)$ and $N(1\to0,j)$ are the number of $0\to1$ and $1\to0$ events in the interval j, counted over the whole trajectory (j has a periodicity of 36). The reported equilibrium constant is then calculated as $K^{\text{rep}}=k_f^{\text{rep}}/k_b^{\text{rep}}$. The rate constants estimated using this procedure, obtained by digitizing figure 5 of ref. 4, are reproduced in Fig. S2. Interestingly, the rates for Cy3-ATP binding in the presence and absence of P_i are indistinguishable from each other within the scatter in the data, as seen in Fig. S2. So, we treat them as essentially identical and compare them later with the same theoretical prediction. A similar remark applies to Cy3-ADP in Fig. S2.

The reported uncorrected experimental rate estimates defined in Eqs. **S1** and **S2** are calculated, for sufficiently long trajectories, from the averaged values,

$$k_f^{\text{rep}}(\theta_j)=N(0\to1,j)/T=\frac{\langle N(0\to1)\rangle_j}{t}, \qquad \text{[S3]}$$

$$k_b^{\text{rep}}(\theta_j)=\frac{\langle N(1\to0)\rangle_j}{\langle t(\sigma=1)\rangle_j}, \qquad \text{[S4]}$$

where the average $\langle\cdot\rangle_j$ is calculated over a single interval j, and all quantities depend on τ, t, k_f, and k_b. The k_f and k_b are the actual θ_j -dependent rate constants, the subject of the present theoretical predictions. In Eq. **S3**, the error due to using T instead of T_0 is also taken into account in the theoretical calculation of uncorrected forward rates, following the procedure used for the experimental estimation of k_f^{rep}.

Assuming steady-state conditions, the probability of being in a state $\sigma=0$ or 1 at any time is given in terms of the rate constants as

$$p_0=k_b/(k_f+k_b), \quad p_1=k_f/(k_f+k_b). \qquad \text{[S5]}$$

The survival probabilities in states 0 and 1, denoted by S_0 and S_1, are both exponential, $S_0(t)=\exp(-k_ft)$ and $S_1(t)=\exp(-k_bt)$, respectively. The probability distributions that the states have lived a lifetime between 0 and t, that is, that it decayed before t, are $[1-S_0(t)]$ and $[1-S_1(t)]$. Their time derivatives, namely the associated probability densities of lifetimes, the so-called waiting time distributions $\rho_0(t)$ and $\rho_1(t)$, are given by

$$\rho_0(t)=k_f\exp(-k_ft), \quad \rho_1(t)=k_b\exp(-k_bt). \qquad \text{[S6]}$$

The probability densities ρ_0 and ρ_1 describe the statistics of times spent in the 0 and 1 states in the trajectories (Fig. S3). We define the local time t as the time relative to the time when the rotor angle reaches the beginning of an interval j. In experiment, the finite acquisition time of video frames and the shot noise limit the effective time resolution. As a consequence, states that seem to be of $\sigma=1$ but are shorter than $\tau=0.1$ s were discarded in the analysis of Adachi et al. (4). We denote by $p(\sigma_0,n)$ the probability of a succession of n events of changed occupancy occurring at times $\{t_1,t_2,\ldots\}$ during any given 10° interval, given the condition of the system's being in occupancy σ_0 at $t=0$. Similarly, the probability that these n events are missed is denoted by $p_{\text{miss}}(\sigma_0,n)$.

The statistics of binding and release events depend on parameters τ and t. In our calculations, τ and t are formally treated as variables and are subsequently assigned the constant values used by the experimentalists, as indicated earlier, so $p(\sigma_0,n)$ and $p_{\text{miss}}(\sigma_0,n)$ are probabilities that depend on these variables τ and t. These probabilities can be cast as expectation values with respect to τ_n s (defined as t_n-t_{n-1} in Fig. S3). As an example, for $n=2$ and $\sigma_0=0$, $p(0,2)=p_0\langle\Theta(t_2<t<t_3)\rangle$ and $p_{\text{miss}}(0,2)=p_0\langle\Theta(t_2<t<t_3)\Theta(\tau_2<\tau)\rangle$. Here, Θ is a generalized Heaviside function which is 1 if the argument is true and 0 otherwise, and $\langle\cdot\rangle$ is a notation for the integration of the enclosed argument with respect to all τ_n s.

In addition to events of the type $p_{\text{miss}}(\sigma_0,2)$, missed "cross-boundary events," denoted by $p'_{\text{miss}}(\sigma_0,2)$, also have a contribution. Missed cross-boundary events are transitions occurring in a bin with the previous or subsequent transition occurring in another interval, and which transitions are missed due to the time

spent between the two events is too short to be resolved. For example, one such event is when a $0\to1$ transition occurs during the j^{th} bin, and the subsequent transition occurs in a subsequent interval, but the time spent in state 1 is too short (i.e., $<\tau$) to be detected. Such $p'_{\text{miss}}(\sigma_0,1)$, formally written as $p_0\langle\Theta(t_1<t<t_2)\Theta(\tau_2<\tau)\rangle$, leads to a convolution integrals. For example, for $\sigma_0=0$, the time-domain expression is $p(0,2|t)=p_0\int_0^\infty\int_0^\infty\int_0^\infty\rho_0(\tau_1)\rho_1(\tau_2)\rho_0(\tau_3)\delta(t-\tau_1-\tau_2-\tau_3)d\tau_3d\tau_2d\tau_1$ and $p_{\text{miss}}(0,2|t)=p_0\int_0^\infty\int_0^\tau\int_0^\infty\rho_0(\tau_1)\rho_1(\tau_2)\rho_0(\tau_3)\delta(t-\tau_1-\tau_2-\tau_3)d\tau_3d\tau_2d\tau_1$ and a Laplace transform $(t\to s,\ \tau\to u)$ formally facilitates their evaluation. For $p(\sigma_0,n)$ the Laplace transform $t\to s$ is a formally simple expression (we use a tilde to denote the transform),

$$\begin{aligned}\tilde{p}(\sigma_0,n|s)&=\int_0^t p(\sigma_0,n|t)e^{-st}dt\\&=p(\sigma_0)\left\langle\exp(-st_n)\frac{1-\exp(-s\tau_{n+1})}{s}\right\rangle.\end{aligned}\qquad\textbf{[S7]}$$

Using $t_n=\tau_1+\ldots+\tau_n$, for $\sigma_0=0$, an analytic expression follows,

$$\tilde{p}(0,n|s)=p(0)\times\begin{cases}\left[\widetilde{\rho_0}(s)\widetilde{\rho_1}(s)\right]^{n/2}, & n\text{ even},\\ \left[\widetilde{\rho_0}(s)\right]^{(n+1)/2}\left[\widetilde{\rho_1}(s)\right]^{(n-1)/2}, & n\text{ odd},\end{cases}\qquad\textbf{[S8]}$$

where $\tilde{\rho}_0(s)=k_f/(s+k_f)$ and $\tilde{\rho}_1(s)=k_b/(s+k_b)$. An expression for $p(1,n|s)$ results by analogy from Eq. **S8** (i.e., by interchanging states 0 and 1).

In the calculation of the probability of the missed events, for each short event an additional condition applies, which is formally achieved by introducing an additional variable. For the leading terms of $n=2$, which provide the most contribution, a single additional variable is needed $(\tau\to u)$, leading to a double Laplace transform,

$$\tilde{p}_{\text{miss}}(0,2|u,s)=p_0\tilde{\rho}_0(s)\tilde{\rho}_1(s)u^{-1}(s+k_f)^{-1}.\qquad\textbf{[S9]}$$

For the cross-boundary missed events,

$$\tilde{p}'_{\text{miss}}(0,1|u,s)=p_0(s\,u)^{-1}\tilde{\rho}_0(s)\left[\tilde{\rho}_1(u)-\tilde{\rho}_1(s+u)\right].\qquad\textbf{[S10]}$$

Again, by analogy expressions for $\tilde{p}_{\text{miss}}(1,2|s)$ and $\tilde{p}'_{\text{miss}}(1,1|u,s)$ follow from Eqs. **S9** and **S10**.

The above Laplace-space expressions are then inverted by elementary inversion, facilitated by the use of symbolic computation tools (37). Of special importance are the one-event contributions,

$$p(0,1)=p_0k_f/(k_f-k_b)\left[\exp(-k_bt)-\exp(-k_ft)\right],\qquad\textbf{[S11]}$$

$$p(1,1)=p_1k_b/(k_b-k_f)\left[\exp(-k_ft)-\exp(-k_bt)\right],\qquad\textbf{[S12]}$$

and the two-event contributions,

$$p(0,2)=-\frac{k_fk_b^2}{(k_f+k_b)(k_f-k_b)^2}\times\left(e^{-k_ft}-e^{-k_bt}+k_fte^{-k_ft}-k_bte^{-k_ft}\right),\qquad\textbf{[S13]}$$

$$p(1,2)=\frac{k_f^2k_b}{(k_f+k_b)(k_f-k_b)^2}\times\left(e^{-k_ft}-e^{-k_bt}+k_fte^{-k_bt}-k_bte^{-k_bt}\right).\qquad\textbf{[S14]}$$

The leading terms that effectively determine the probability of missed events within an interval are

$$\begin{aligned}p_{\text{miss}}(0,2)=&k_fk_b^2e^{-k_ft-k_b3\tau}(\mathrm{k_f}+k_b)^{-1}(k_f-k_b)^{-2}\\&\left(e^{k_f3\tau}-e^{k_b3\tau}+k_fte^{k_f3\tau}-k_fte^{k_b3\tau}\right.\\&\left.-k_bte^{k_f3\tau}+k_bte^{k_b3\tau}-k_f3\tau\,\mathrm{e}^{k_f3\tau}+k_b3\tau\,e^{k_f3\tau}\right).\end{aligned}\qquad\textbf{[S15]}$$

For the cross-boundary missed events, the Laplace inversion yields for the leading terms

$$\begin{aligned}&p'_{\text{miss}}(0,1)+p'_{\text{miss}}(1,1)=\\&\left[e^{-k_ft}e^{-k_b3\tau}-e^{-k_b3\tau}-\frac{k_fe^{-k_ft}}{k_f-k_b}+\frac{k_fe^{-k_bt}}{k_f-k_b}\right.\\&\left.+k_fk_be^{-k_b3\tau}\left(\frac{1}{k_fk_b}+\frac{e^{-k_f(t-3\tau)}}{k_f(k_f-k_b)}-\frac{e^{-k_b(t-3\tau)}}{k_b(k_f-k_b)}\right)\right].\end{aligned}\qquad\textbf{[S16]}$$

To obtain the reported rates from Eqs. **S3** and **S4** we subtract the probability of missed events from the total probability of events,

$$\begin{aligned}k_f^{\text{rep}}(\theta)\cong t^{-1}[&p(0,1)+p(0,2)+p(1,2)\\&-p_{\text{miss}}(0,2)-p'_{\text{miss}}(0,1)-p'_{\text{miss}}(1,1)],\end{aligned}\qquad\textbf{[S17]}$$

$$\begin{aligned}k_b^{\text{rep}}(\theta)&\cong(tp_0)^{-1}\langle N(1\to0,\tau,t)\rangle_j\\&=(tp_0)^{-1}[p(1,1)+p(1,2)+p(0,2)\\&\quad-p_{\text{miss}}(0,2)-p'_{\text{miss}}(0,1)-p'_{\text{miss}}(1,1)].\end{aligned}\qquad\textbf{[S18]}$$

In the calculations we neglect higher-order contributions (i.e., terms where $n\geq3$). This approximation is valid if t is smaller or comparable with the inverse of the rates, that is, $t\leq1/k_f$ and $t\leq1/k_b$. In our calculations it is always verified that this condition is met. We note that the definitions in Eqs. **S1** and **S2**, for sufficiently slow rotation, yield $k_f^{\text{rep}}<k_b^{\text{rep}}$, even if the actual rate constants have the opposite relation, $k_f>k_b$. Thus, the latter condition could effectively be masked in the experiments, but with the necessary corrections the actual rates can be recovered. As discussed in the text, the number of missed $0\to1\to0$ events is appreciable at low θ values, that is, at $\theta\sim-50°$, when k_b becomes large compared with $1/t$ and much larger than k_f, resulting in significant corrections for both k_f and k_b, as seen in Fig. S4. The same remark applies to $0\to1\to0$ events, when $k_f>1/t$ and $k_f\ll k_b$, but these conditions are not reached in the experiments.

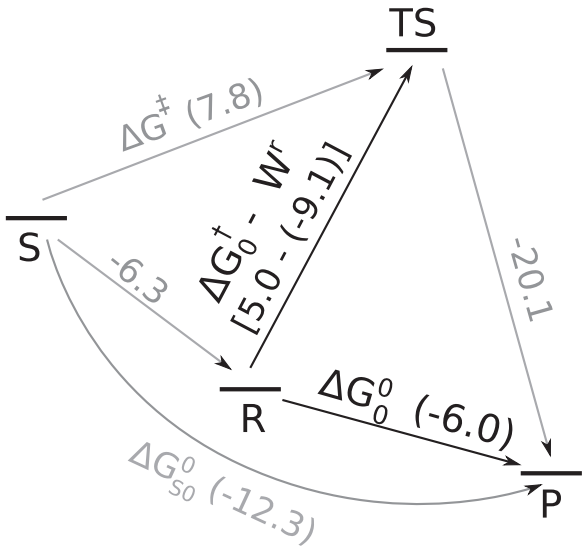

Fig. S1. Diagram of free energy changes (in units of kilocalories per mole) with values provided for the case of free rotation. The three quantities W^r, $\Delta G_0^{\dagger}$, and ΔG_0^0 that yield $\alpha(0)$ and λ are shown in bold. Other free energy terms used to calculate these three quantities are shown in light type.

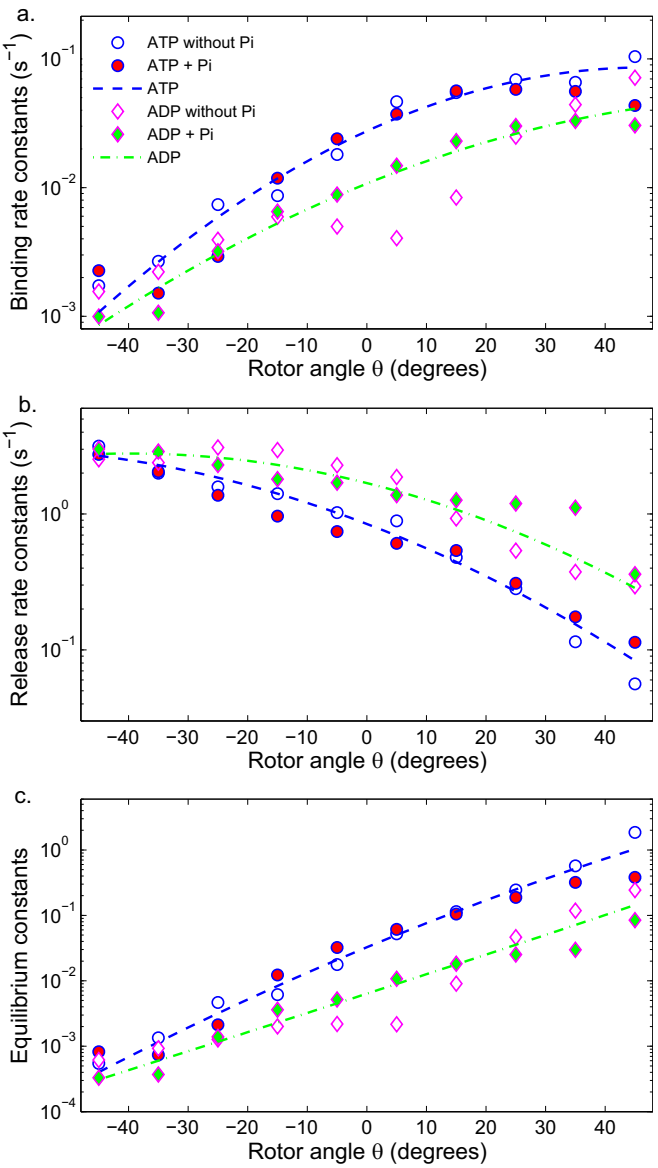

Fig. S2. Reported binding (*A*) and release (*B*) rate constants and equilibrium rate constants (*C*) vs. rotor angle θ in the range −50° to 50°, extracted by Adachi et al. (4) from controlled rotation experiments for the fluorescent nucleotides. Open symbols denote the nucleotide (circle for ATP and diamond for ADP) binding and release without P_i in solution, and closed symbols denote the presence of P_i in solution. The lines are a smooth fit to the ATP and ADP data points.

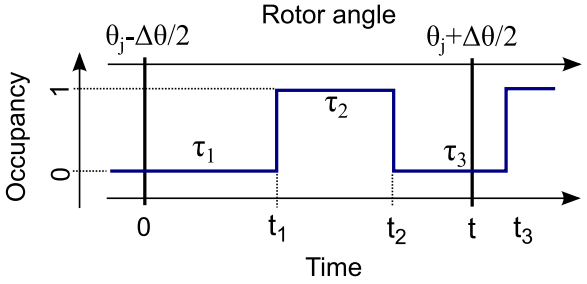

Fig. S3. Example of occupancy change event series described by probability $p(0, 2|t)$ (Eq. **S13**) and related text for definitions) in the j^{th} interval corresponding to a rotation of constant rate from angle $\theta_j - \Delta\theta/2$ to angle $\theta_j + \Delta_\theta/2$. A two-state rate model with rate constants k_f and k_b describes the kinetics of jump events.

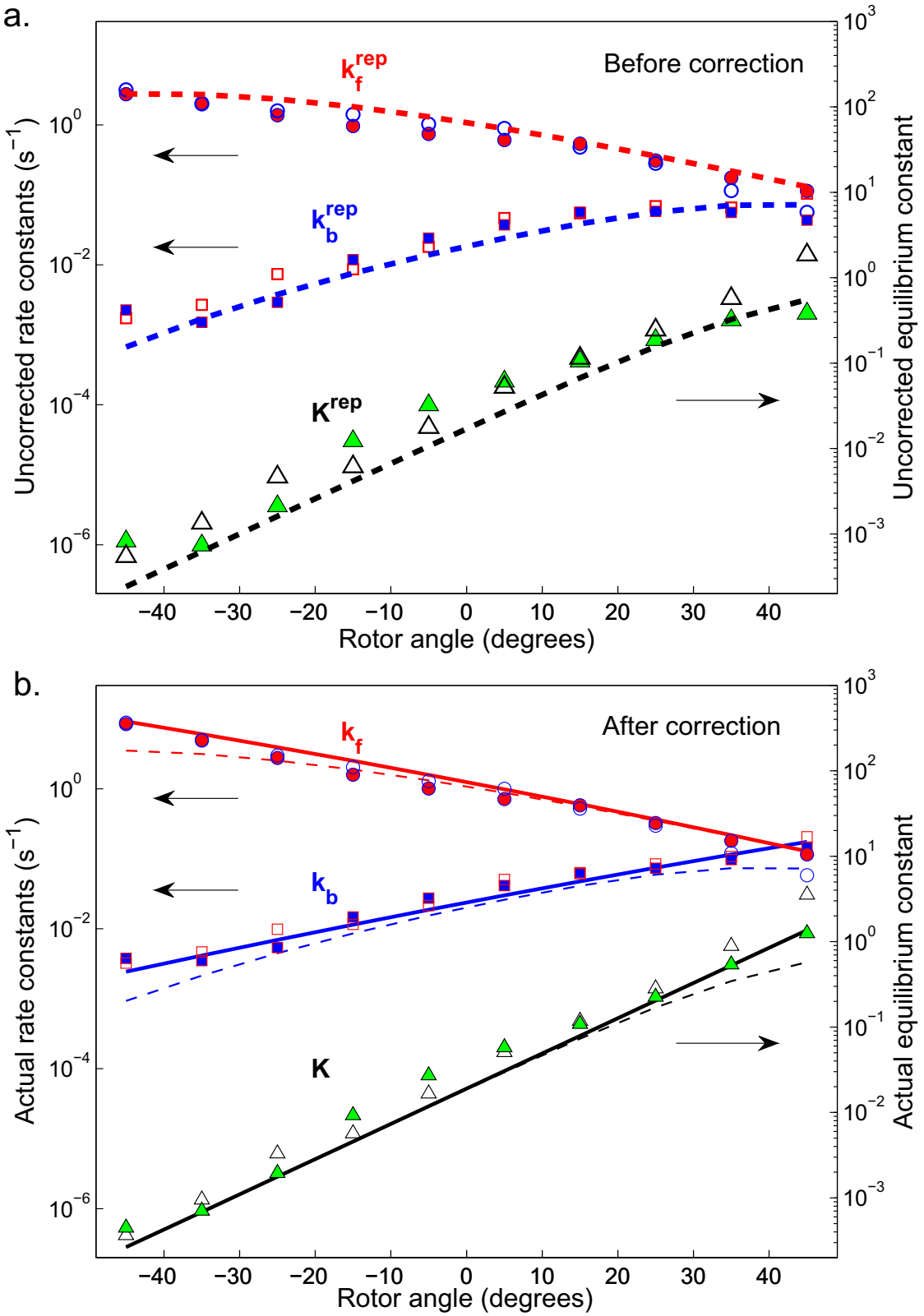

Fig. S4. Reported (*A*) and corrected (*B*) binding and release rate constants and equilibrium rate constants vs. controlled rotation angle for fluorescent ATP in the presence (solid symbols) and absence of P_i (open symbols) in solution. *B* is identical to Fig. 2 in the main text. The reported uncorrected experimental data are compared with their theoretical counterparts by calculating missed events and also correcting for an error due to replacing T_0 by T. Squares, circles, and triangles are experimental points, and solid lines are theoretical values. Dashed lines in *A* and *B* show the theoretical data without corrections.

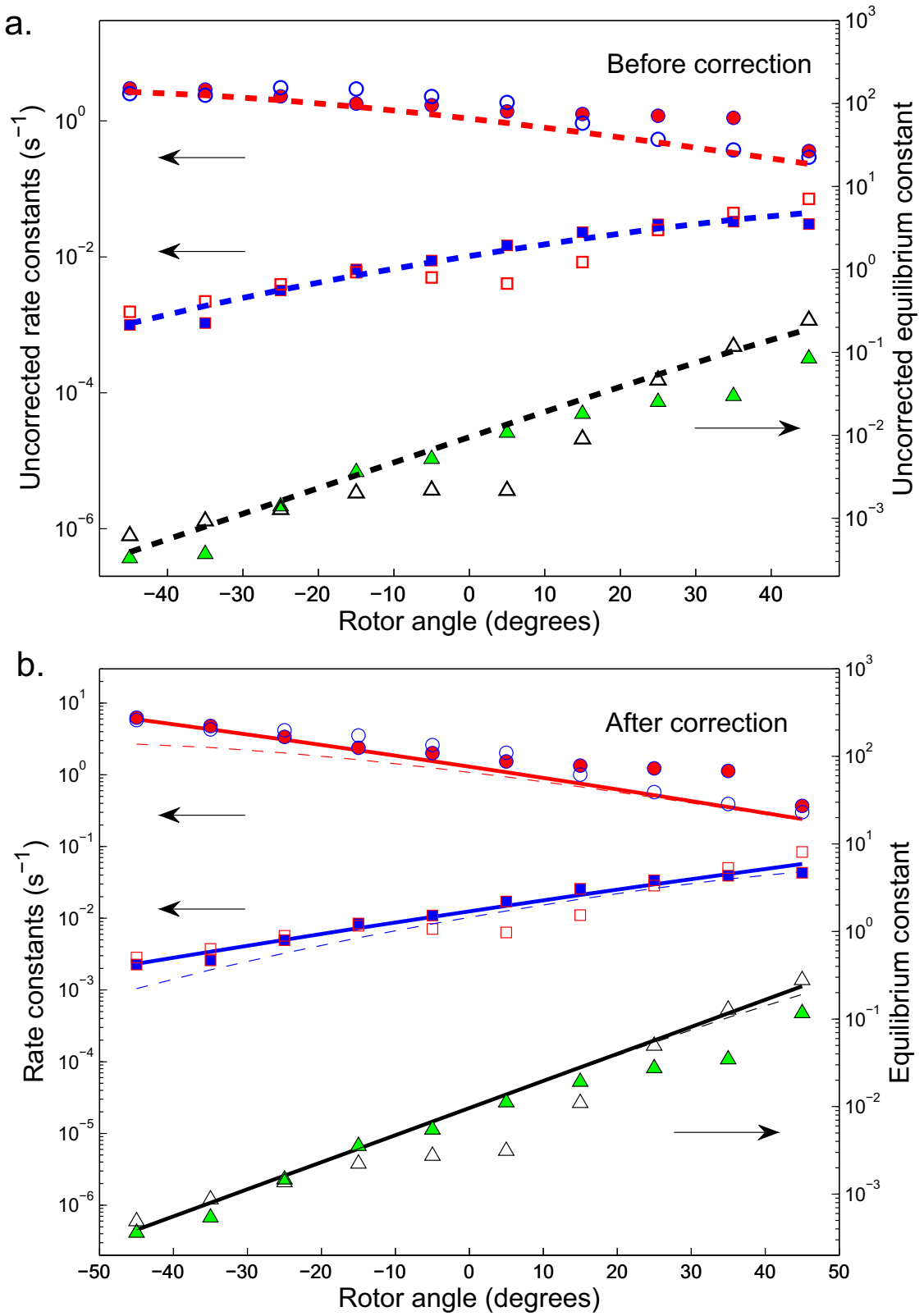

Fig. S5. Reported (*A*) and actual (*B*) binding and release rate constants and equilibrium rate constants for Cy3-ADP in the presence and absence of P_i in solution. *B* is identical to Fig. 3 in the main text. The theoretical curves for $\ln K^{rep}$ vs. θ were fitted to experiment, which yielded $\kappa^{ADP} = 12$ pN·nm/rad^2 and $k_f^{ADP}(0) = 4.6 \times 10^6$ M^{-1}·s^{-1} $= 0.5 \cdot k_f^{ATP}(0)$.